GPS Diffractive Reflectometry: Footprint of a Coherent Radio Reflection Inferred From the Sensitivity Kernel of Multipath SNR

Felipe Geremia-Nievinski, Matheus Ferreira e Silva, Karen Boniface, *Member, IEEE*, and João Francisco Galera Monico

***Abstract*—The validation of remote sensing environmental estimates requires knowledge of their spatial extent and resolution. Here, we consider coherent radio reflections routinely observed in ground-based global positioning system (GPS) reflectometry. Their footprint is often conceptualized in terms of the specular point (SP) and the first Fresnel zone (FFZ). Such infinitesimal point and finite zone can be generalized into a spatially continuous sensitivity kernel (SK). The SK represents a diffraction pattern, as the importance of each surface portion depends on its scattered field contribution in power and phase. We measured the SK of a GPS radio reflection under bipath reception conditions. The SK exhibited oscillations along the plane of incidence. The envelope of oscillations peaked near the SP and persisted in its decay well beyond the FFZ. Within the FFZ, sensitivity was skewed toward the antenna. This experiment suggests the feasibility of overcoming the diffraction limit and resolving features smaller than the FFZ with the exploitation of GPS diffraction patterns.**

***Index Terms*—Coherent, global navigation satellite system (GNSS), global positioning system (GPS), multipath, reflection, reflectometry.**

I. Introduction

SPACEBORNE environmental monitoring typically needs ground-based measurements for calibration and validation [1]. The comparison of different types of retrievals requires harmonizing their spatial extent and resolution, up- or downscaling as appropriate [2]. This requirement translates in the specification of the footprint sampled by remote sensors and *in situ* probes [3].

Here, we investigate global positioning system reflectometry (GPS-R) applications, which have been demonstrated from space, air, sea, and land platforms; see [4] and [5] for general reviews. Especially near-surface or close-range GPS-R has proved its technical readiness for long-term monitoring of a variety of environmental parameters, such as soil moisture, snow depth, vegetation growth, and sea level; see [6] for a more specific review. Few-meter-tall GPS-R antenna tower or monument installations offer environmental estimates at an intermediate spatial scale ($\sim$100 m radius), bridging the gap between far-range sensors ($\sim$km pixels in satellite imagery) and contact measuring devices ($\sim$ cm terminals buried in soil).

We narrow our scope first by considering GPS-R observations where stable-phase or coherent specular reflections predominate [7]–[12]; this is in contrast to GPS-R in the incoherent scattering regime, for which effects such as speckle are undesirable and averaged out through intentional randomization. Second, we concentrate on bi- or multi-path reception conditions, whereby a few propagation paths—the line-of-sight (LOS) or direct one and its reflections (non-LOS, NLOS)—are left to interfere naturally with each other prior to sampling and then tracked in combined form via correlation against a single replica [13], [14]. Similar constructive/destructive interference could also be achieved artificially, by complex correlating the direct and reflected signals after they had been tracked separately against their own replicas; this two-replica mode may employ one or two antennas, depending on how well the two paths are separated in ranging delay and/or direction of arrival, although that is often difficult near grazing incidence. Third, while the single-replica single-antenna mode considered here—referred to as GPS multipath reflectometry (GPS-MR)—may produce various observables (pseudorange, carrier-phase, and signal-to-noise ratio or SNR; each reported just at peak correlation or over a varying delay waveform or delay-Doppler map), we focus on peak SNR. (Phase-based GPS-MR has been reported in, e.g., [15] and [16]; for pseudorange-based GPS-MR, see [17].) SNR-based GPS-MR, also known as GPS interference pattern technique (GPS-IPT [18]) or GPS interferometric reflectometry (GPS-IR [6]), is analogous to Lloyd's mirror in optics [19] and to the early sea-interferometers used in radio astronomy [20], [21].

Manuscript received August 3, 2015; revised February 2, 2016 and April 4, 2016; accepted May 24, 2016. Date of publication July 19, 2016; date of current version October 14, 2016. This work was supported in part by the Brazilian National Council for Scientific and Technological Development (Award 457530/2014-6). Some of this material is based on data, equipment, and engineering services provided by the Plate Boundary Observatory operated by UNAVCO for EarthScope (http://www.earthscope.org) and supported by the U.S. National Science Foundation (EAR-0350028 and EAR-0732947). *(Corresponding author: Felipe Geremia-Nievinski.)*

F. Geremia-Nievinski was with the Faculty of Sciences and Technology, São Paulo State University, Sao Paulo 19060-900, Brazil. He is now with the Department of Geodesy, Federal University of Rio Grande do Sul, Porto Alegre RS 91501-970, Brazil (e-mail: fgnievinski@gmail.com).

M. F. Silva is with the Faculty of Sciences and Technology, Sao Paulo State University, Sao Paulo 19060-900, Brazil (e-mail: matheus92ferreira@gmail.com).

K. Boniface is with the Univ. Grenoble Alpes, ISTerre F-38041 Grenoble, France (e-mail: karen.boniface@gmail.com).

J. F. G. Monico is with the Faculty of Sciences and Technology, São Paulo State University, Sao Paulo 19060-900, Brazil (e-mail: galera@fct.unesp.br).

This paper has supplementary downloadable multimedia material available at http://ieeexplore.ieee.org provided by the authors. This supplementary file has an appendix containing data processing details and auxiliary analyses supporting the main conclusions presented in the body of the article. The total size of the file is 358 KB.

Color versions of one or more of the figures in this paper are available online at http://ieeexplore.ieee.org.

Digital Object Identifier 10.1109/JSTARS.2016.2579599

The footprint of a coherent reflection is often conceptualized in terms of the specular point (SP) and the Fresnel zones (FZ), defined in terms of the propagation delay with respect to the direct path. The first FZ (FFZ), the scattering region delayed up to half wavelength, is even associated with "the thickness of the physical ray" [22]. This picture is in contrast to geometrical rays in the limit of infinite frequency carrier waves. For example, in [18] the SP is employed to interpolate individual GPS-R soil moisture retrievals to produce a gridded map; in [23] the FFZ serves as a convolution kernel for interpreting the signature of buried objects; [24] used SP to determine whether sea reflections were blocked by the presence of ships; [25] utilized FFZ to conclude that surrounding trees were out of the coverage of the GPS footprints.

The sensitivity kernel (SK) generalizes the infinitesimal SP and finite FZ into spatially variable weights. It quantifies the importance of each surface portion with due consideration for their power and phase contribution, resulting in a continuous surficial field instead of an all-or-nothing spatial mask. The formation of an individual specular reflection on a planar surface has to consider diffraction effects, as it involves the coherent superposition of countless physical wavelets (Huygens principle [26]). In this approach, we exclude from consideration additional specular reflections possible on a non-planar surface.

Previous work related to SK in general and diffraction in specific has been reported across several disciplines. In the fields of seismology and acoustics, the SK has received considerable attention for wave reflection and propagation [27], [28], with more recent works quantifying the SK experimentally [29], [30], as we do here for radio waves. In electrical engineering, the intentional manipulation of odd and even FZ is a common antenna design technique [31]. In the assimilation and inversion of atmospheric and seismic data, the SK is a key component for obtaining the averaging kernel of an observation system, thus quantifying the information content contributed by observations [32], [33]. In general optics, diffraction by a fixed aperture as observed from varying directions [26] represents the primal problem whose dual is considered here, of a fixed observation direction and varying aperture location.

In GPS positioning, where multipath reception conditions are undesirable, a related diffraction phenomenon is often observed in partially obstructed LOS propagation [34], [35], although it has not been linked to partial or FFZ-incomplete reflections in the way done here. In GPS-R, focus has been on the footprint of incoherent bistatic scattering, possibly pulse- and beam-limited, which may be imaged in terms of delay-Doppler maps; it follows from a multitude of distinct geometrical optics (GO) reflections, where FFZ-scale diffraction is typically negligible [36], [37].

In the context of SNR-based GPS-MR and with the goal of determining its sampling footprint, we report on the very first experimental results measuring the SK of an oblique-incidence coherent reflection as observed under multipath reception conditions with L-band GPS radio signals ($\sim$20 cm wavelength). These unique measurements are based on the insertion of a localized probe at varying locations over an otherwise unperturbed reflecting surface; simulations are based on physical optics. In the next section, we present the experimental and theoretical methodology, employed to produce results presented and discussed subsequently in Section III. We finalize in Section IV considering the implications for calibration and validation of GPS-MR retrievals as well as prospects for novel sensing capabilities employing diffraction patterns in GPS-R. The Appendix (supplementary material) provide supporting information with details of the data processing and simulation methods.

II. Methods

SNR is the raw GPS observable considered in this paper. It is proportional to measured total power P, which follows from a bipath propagation channel. The first or direct path is along the LOS between spaceborne transmitter and ground-based receiver. The second or reflected path impinges on Earth and scatters away, a part of which is intercepted by the receiving antenna. Both in measurements and simulations, here we consider coherent scattering conditions, producing a stable phase relationship between first and second paths.

The GPS receiver matches direct and reflected paths against a single clean code replica, thus bipath total power $P = P_d + P_r + 2\sqrt{P_d}\sqrt{P_r}\cos\varphi_r$ follows from a complex sum, depending not only on direct power P_d and reflected power P_r but also on their phase difference $\varphi_r = \phi_r - \phi_d$. Notice that the direct phase ϕ_d cancels out in SNR, which is fortunate as it is affected by several poorly known effects along the satellite-to-receiver link (atmospheric delays, clock errors, etc.) [38]. The reflected-minus-direct phase $\varphi_r \approx k\tau$ (where $k = 2\pi/\lambda$) is dominated by the specular delay (neglecting surface material and antenna contributions), which for a horizontal surface is simply $\tau = 2H\sin e$ [39], in terms of the antenna-to-surface reflector height H and the satellite elevation angle e.

The basic scenario above was modified as follows. Both reflector height H and satellite elevation e remained unchanged, while the otherwise unobstructed ground reflection was perturbed with the insertion of a localized probe at varying locations over the ground. The resulting profile of measured total power versus probe location represents the SK of multipath SNR measurements. The reflecting surface was made of a very large horizontal dielectric plane (a concrete parking lot) upon which a small metallic disk (radius $\sim$50 cm) was overlaid (see Fig. 1). Scattering off metal reverses circular polarization, while that off dielectrics has a mixture of both same- and opposite-sense circular polarization [13], [43]. So the disk-over-ground configuration acted as a screen aperture as seen by a co-polarized antenna; i.e., the metal cross-polarized scattering practically nullified the contribution from the covered portion of the ground. Now we describe the measurement and simulation systems.

A. Measurement Setup

A GPS-like right-handed circularly polarized (RHCP) broadcast was provided by a space-based wide-area augmentation system (WAAS) satellite (identifier Anik F1R, PRN 138, longitude 107.3° W). In contrast to regular GPS satellites which rise and set in the sky, this geostationary satellite was visible at a fixed direction in the sky ($\sim$45° elevation angle). A geodetic

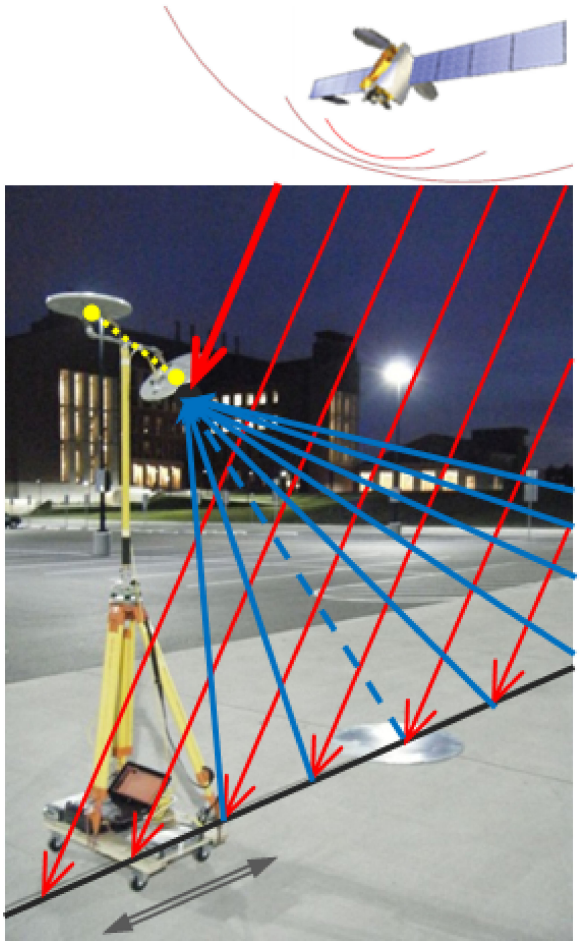

Fig. 1. Cartoon representation of the observation setup. A vertical platform (tripod on left side) includes two independent GPS antenna-receiver sets: up-looking for positioning and down-looking for reflectometry; there is a vector offset between the two (yellow dotted line). A GPS satellite at the top-right broadcasts a wave arriving with planar front and parallel rays (red lines), which is directly incident on the antenna (thick red line). The broadcast also impinges everywhere on the surface (thin red lines; for clarity, only the plane of incidence is highlighted). Scattering follows in all directions, a portion of which is intercepted by the sensing antenna (blue solid lines). A metal disk placed on the surface suppresses the reception of scattering that would have originated at the covered location (blue dashed line).

GPS receiver (Trimble NetR9) was set up to track the latest modernized L5 signal [40] (see below for a paired setup). WAAS satellites do not broadcast L2, and compared to L1, the L5 one features a longer modulation code, improving isolation from simultaneous broadcasts from other GPS satellites [41]. A predominantly RHCP receiving antenna (Trimble Zephyr geodetic II [42]) was positioned $\sim$1.5 m high and pointed with boresight toward the nominal SP (at -45° angle), to boost the reflection reception. The left-handed circularly polarization (LHCP) nullification is at 16 dB level, which is the antenna polarimetric power ratio near boresight. The antenna broad hemispherical gain pattern allowed the simultaneous reception of the direct propagation as well. Such bipath reception conditions permitted the two paths to interfere constructively and destructively, depending on their relative power and phase.

The metal disk was thin ($< \sim$1 mm) and flush with the ground. The antenna–disk pair was deployed along the plane of incidence (spanned by surface normal and satellite LOS) at various horizontal separations (from $\sim$0 up to $\sim$10 m), crossing the SP (at $\sim$2 m). Displacing the antenna minimized undesired disturbances in the scattering conditions, as the metal probe could be left stationed and with no attached devices. The platform was moved manually back and forth, repeating the 10 m traverse 13.5 times during 17 min.

The antenna–disk separation was monitored with a positioning system attached to the sensing antenna (see the Appendix for details). Accordingly, there were two electrically uncoupled GPS antenna-receiver sets, identical except for their antenna orientation (up- versus down-looking). Temporal and spatial repetition allowed randomization of uncorrelated noise. The first and last 25-cm were discarded as the platform was subject to jerk from stopping then returning in the opposite direction (with no rotations).

B. Simulation Outline

We adopted the Physical Optics (PO) high-frequency surface scattering method [44] to examine the formation of a single GO reflection in terms of surface scattering, see integration in (2) of the Appendix. Grid spacing (quarter-wavelength, with $\lambda = 25.5\,\text{cm}$) and limits ($[-11\,\text{m}, +1\,\text{m}]$ and $[-1\,\text{m}, +1\,\text{m}]$, in north and east coordinates) were chosen so that they did not affect simulations. This numerical method is not unlike the faceted approach of [45] and differs from the coherent power implementation of [46] in that we account for phase thus interferometric interactions are allowed.

The integration of PO element-wise scattered electric field contributions results in the PO net scattered field, as an approximation for the GO reflection. The specular delay is replaced for the bistatic delay (see the Appendix); in any case, the direct phase ϕ_d remains inconsequential, as common terms cancel out when differenced. Diffraction effects near the SP can be calculated to first order by simply truncating the surface integral [44], [47]. We checked the unobstructed-case PO integral extensively against an analytical closed-form GO solution [48], which assumes an infinite surface via the stationary phase method [49]. We also checked the obstructed case implementation, though more limitedly, against the method of moments in the FEKO package [50].

III. Results

Here, we present measurement and simulation results.

A. Measurements

Fig. 2 shows the main experimental result (diffraction pattern, DP): measured total power variation as a function of horizontal distance between receiving antenna and metal disk probe. The DP exhibits peaks and troughs, with a main lobe located within the FFZ. The greatest sensitivity was found in the vicinity of the FFZ center and the SP. The envelope of oscillations decays rapidly toward the antenna and more gradually away from it.

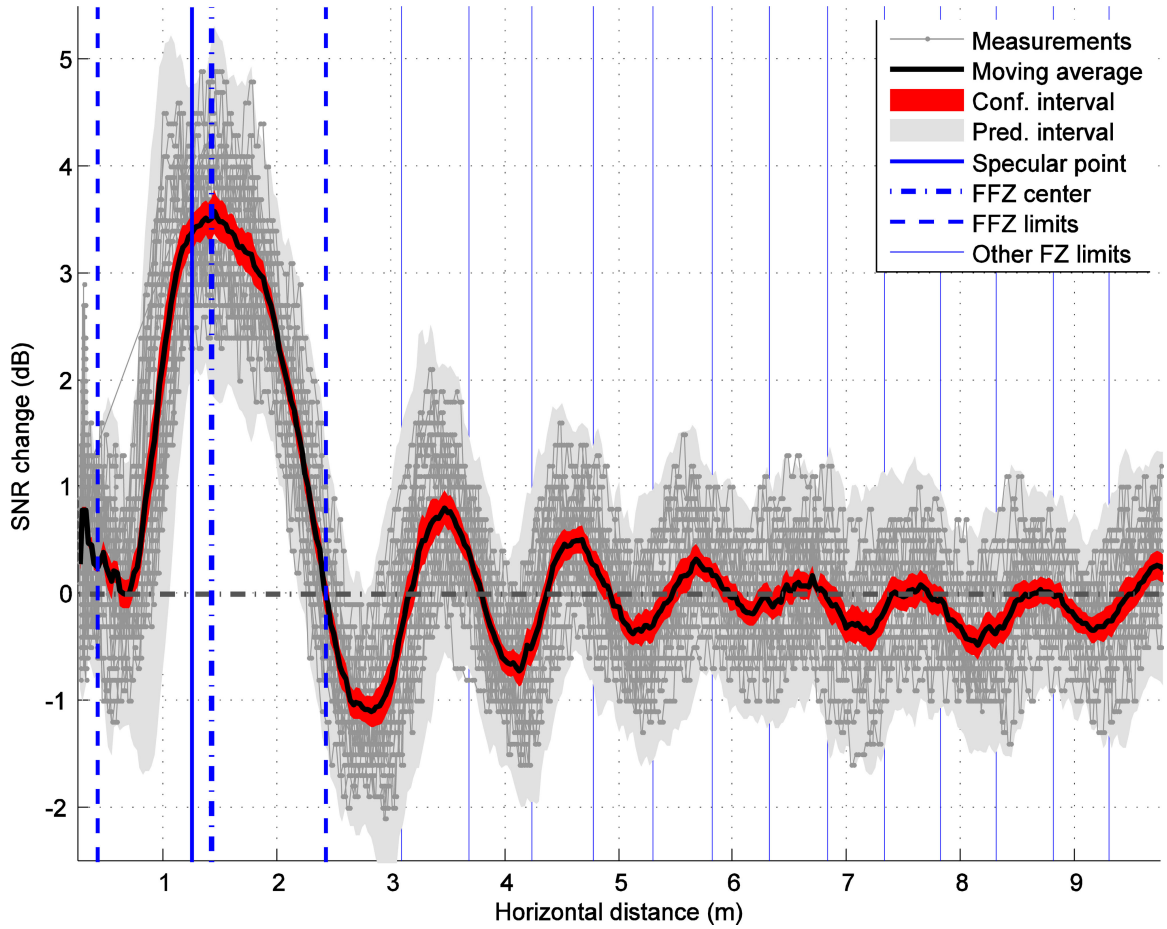

Fig. 2. Measured power variations as a function of horizontal distance between receiving antenna and metal disk probe. Independent SNR measurements are shown as gray dots. A moving-average estimate is shown as a solid black smooth curve; 99% confidence and prediction intervals are shown, respectively, as red and gray bands. The SP is shown as a vertical solid blue line. The FFZ center and inner/outer limits are shown, respectively, as a dashed-dotted and dashed vertical blue lines; subsequent Fresnel zone outer limits are shown as thin blue vertical lines.

Several cycles of significant oscillations are observed farther from the FFZ. Within the FFZ, its near and far ends are asymmetric. Smaller distances, up to the metal disk radius of 46.9 cm +/- 0.3 cm, have to be considered with caution, as the platform was then partially obstructing the disk.

Each gray point represents an independent SNR measurement. No outliers were found nor discarded within the selected 15-min window. The solid black smooth curve is a moving average, calculated with 2.5 cm post spacing and 5-cm-wide overlapping windows. A 99% confidence interval for the mean and 99% prediction interval for observations are shown as red (darker) and gray (lighter) bands, respectively; the former is akin to the standard error of the mean thus it shrinks with increasing point density (contrary to the standard deviation, used in prediction intervals), and may be optimistic because of neglected serial correlation. Vertical lines are drawn at distances corresponding to the following locations: the SP; the FFZ center and limits (inner/outer ends of the ellipse); and the *i*th Fresnel zone outer limit (up to 15th FZ).

To isolate the power variations, a constant 41 dB was subtracted from SNR values, as a representative value of the unobstructed conditions; it was obtained as the median SNR of obstructed conditions excluding the main lobe. Ideally, it would have been the average SNR of unobstructed conditions measured at exactly the same antenna height. An error in this constant would not affect the DP other than shifting it up or down as a whole. The algebraic sign of SNR differences was reversed for improved visualization.

The horizontal distance at which the reference vertical lines were drawn depends on the satellite direction (primarily elevation angle and secondarily azimuth, if the surface is nonhorizontal), antenna position, and surface tilting. Satellite remained stable at 43.7° elevation and ∼183° azimuth during the observation period. The horizontal position uncertainty was at few-cm level for relative positions and several centimeters in absolute sense; the latter includes uncertainties in the offset between up- (positioning) and down-looking (sensing) antennas; see the Appendix for details. The dissimilar relative and absolute uncertainties mean that the shape of the DP is susceptible more to shifting than to stretching left-to-right in Fig. 2, i.e., an additive bias in the abscissa is more likely than a multiplicative distance error. The antenna vertical position uncertainty was also centimetric, and it was subject to a small surface slope (see the Appendix for details). These factors lead to an uncertainty

propagation approaching one decimeter for the location of SP and FFZ center; care must be exercised in their interpretation.

B. Simulations

Fig. 3 shows a simulated DP: total power variation as a function of horizontal distance between receiving antenna and metal disk probe. There is excellent agreement with experimental results (see Fig. 2), in terms of the oscillatory behavior, including the main lobe within the FFZ and the number of cycles. The foreground red thick curve (darker) represents the average of individual simulation runs (gray thin curves). To quantify the variability of results due to the centimetric positional uncertainty mentioned above (details in the Appendix), the simulation is repeated shifting the antenna vertically and horizontally, respectively, in three and five 2.5-cm steps—in total, 15 shift combinations within a box 12.5×7.5 cm. Each curve is made of one hundred 10-cm spaced dots, and each dot is obtained solving the two-dimensional PO integral as per (3) in the Appendix.

The zero-fixing constant SNR value was obtained simulating unobstructed conditions. Accounting for a small surface slope ($\sim 1\,\mathrm{cm/m}$) improved the agreement in the relative position of zero-crossings, compared to measurements. The envelope of oscillations agrees less favorably: a constant 3 dB empirical power factor was added to Fig. 3 (both green and red traces) so as to bring it to ordinate scale of Fig. 2, i.e., we had to correct the global scale of simulated power oscillations *a posteriori* vis-à-vis measured ones; this is likely because of imperfect reflection coefficients. Localized discrepancies persist, especially in the nearest and farthest distances; e.g., the part closest to the antenna and up to SP distance was found especially reactive to the LHCP broadcast component (this follows from the antenna non-negligible LHCP gain away from boresight, a region exposed due to the antenna orientation) and also the receiving antenna polarimetric phase difference. Nonetheless, the essential features of the measured DP are well represented in the simulation results.

The green line in Fig. 3 represents the power variation that would be observed if the region outside of the FFZ were truly negligible. In this case, the oscillatory DP is replaced with a more triangular distribution, exhibiting decaying sensitivity as the metal-overlapped area shrinks, and eventually attaining insensitivity as soon as the probing disk ceases contact with the FFZ. This simplified case disagrees with measurements as well as with the realistic simulation.

C. Discussion

As illustrated in Fig. 4 of Appendix, the DP can be modeled as an oscillating trigonometric factor $\cos\dot{\varphi}$ (with phase $\dot{\varphi}$) whose amplitude is modulated by an envelope $2\sqrt{\dot{p}}$ (with power $\dot{p}$), please see (4)–(9) in the Appendix for notation. The relative phase $\dot{\varphi}$ (that of the obstruction compared to the unobstructed scenario) is dominated by the bistatic propagation delay—which is greater than the specular delay (SD)—experienced at each surface portion. The relative power $\dot{p}$ (obstruction versus unobstructed conditions) produces the trend-plus-envelope combination $\dot{p} + 2\sqrt{\dot{p}}$ (dark green trace in Fig. 4 of Appendix) that serves to establish a cutoff distance for non-negligible surface scattering contributions; for example, the 95% SNR cutoff (5% of SNR maximum, 1.75 W/W) is located at the distance of 4.60 m (thick blue vertical line in Fig. 4 of Appendix), near the 5th FZ's limit. Repeating the simulation for more typical conditions (upright antenna over a soil surface and substituting the metal disk with an aperture) reduces the peak contrast markedly (0.25 dB instead of 4.0 dB SNR change) and enlarges the 95% cutoff distance ($\sim$6.5 m, past the 8th FZ); the distance increases with decreasing peak contrast because the DP envelope also becomes broader (peak contrast decreased in the first place because the antenna is no longer pointed at the SP).

Furthermore, the fact that sensitivity is not greatest immediately under the receiver (where free-space power loss is least) suggests that proximity is a secondary effect; instead, bistatic phase variation might be the dominating effect, a consequence of bistatic delay being stationary at the SP. Indeed, simulations for an antenna twice as high (not shown), still put the 95% cutoff distance past the 10th FZ. This interpretation can be substantiated in terms of the Fraunhofer approximation, in which the obstruction phasor $\sqrt{\dot{p}}\angle\dot{\varphi}$ follows from a complex-valued integral over the disk area, assuming uniform magnitude and bilinear phase variation, which results in a sinc function favoring regions of slow phase variation.

Another inference permitted by these findings follows from the Huygens principle, in that even for a specular reflection on a planar surface, the reflected signal is the net effect of coherent scattering originating at bistatic delays not only equal to but also greater than the specular delay (SD). This feature could be exploited via correlation-versus-delay waveforms (DW), defined as the so-called delay-Doppler map sliced or collapsed for constant Doppler and varying time-delay. Although the GPS receiver we employed records just peak-correlation SNR, the lack of delay diversity (compared to using a full DW profile) could be compensated by additional spatial diversity so as to sample the wavefront, e.g., using vertically and horizontally displaced antennas. As each scalar SNR measurement is the outcome of convolution between the SK reported here against the reflecting surface conditions, knowledge of the SK would allow recovering unknown surface scattering features, under redundant observation geometry (i.e., with more observations than unknowns). This prospect, for extending GPS-IPT/IR into a new GPS Diffraction Pattern Technique or GPS Diffractive Reflectometry (GPS-DPT/DR), is analogous to the exploitation of DP for probing and imaging small targets with large-wavelength radiation, commonplace in other parts of the spectrum. It would consist in collecting a series of SNR measurements using an array of GPS receivers/antennas, followed by special data processing for inverting their SK matrix (notwithstanding regularization and constraining to mitigate possible ill-conditioning).

Even if not trying to map out surface features smaller than the FFZ as proposed above, knowledge of the SK serves to guide the interpretation of average surface condition retrievals, such as site-wide snow depth and soil moisture. It should be recalled that conventional SNR-based GPS-MR does not work with isolated SNR values, rather employs a series of measurements collected from a given reflector height H_0 and over a range of satellite

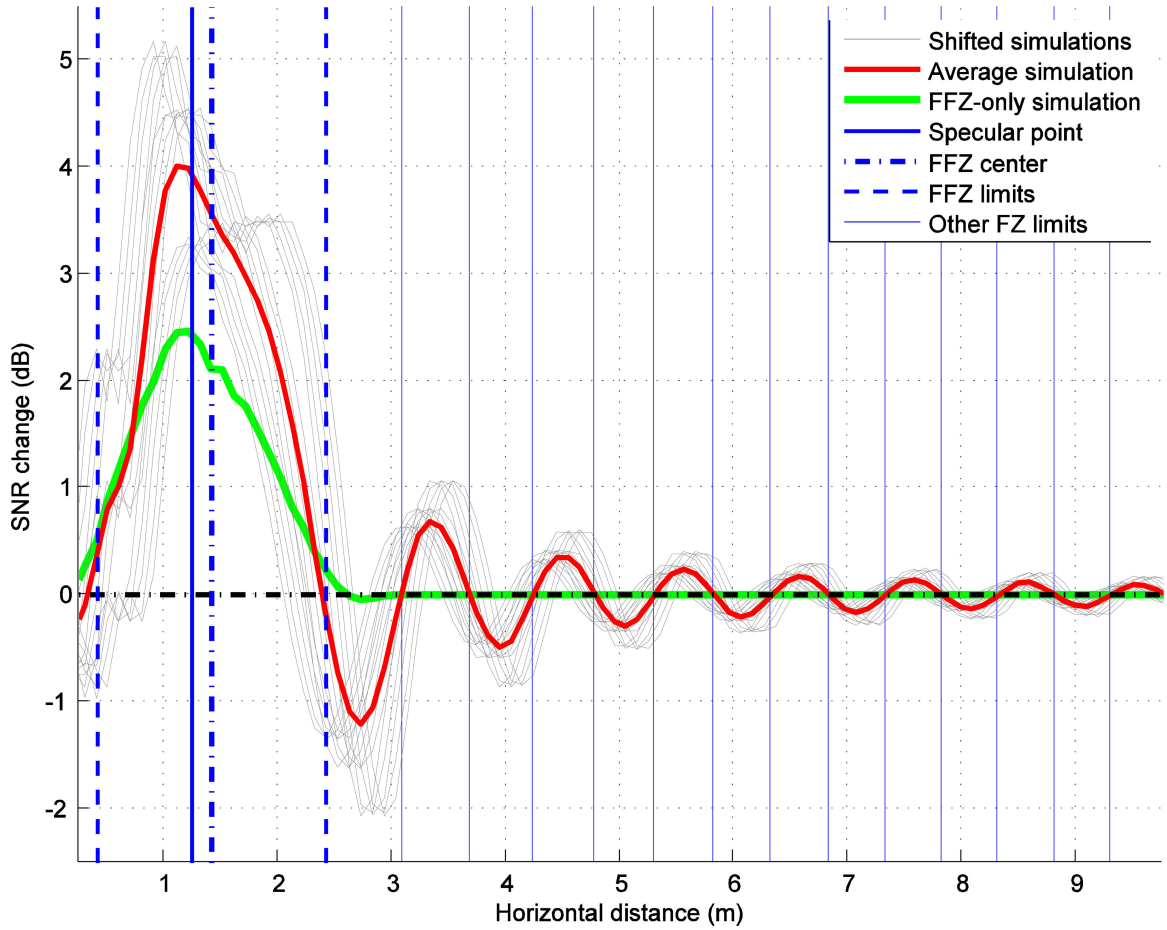

Fig. 3. Simulated power variations as a function of horizontal distance between receiving antenna and metal disk probe. Individual simulation runs are shown as gray thin curves and their average as a red thick curve. A simulation considering only the FFZ is shown as a green triangular line. Vertical lines are as in Fig. 2.

elevation angles $e_1, e_2, \ldots$, which can be as wide as several tens of degrees ($5^\circ \leq e \leq 35^\circ$) or more. Evidently, the SK would change with elevation, basically with the DP envelope accompanying the FFZ (that moves and resizes over the ground) and with DP oscillations cycling (according to bistatic delay). The multiple single-elevation SK involved would have to be propagated so as to produce the SK of a particular scalar observable (e.g., best-fitting sinusoid frequency, phase-shift, or amplitude) extracted from the SNR measurement vector.

As future work, carrier-phase and pseudorange-based GPS-MR could be considered in addition to SNR (GPS-IPT/IR). Second, one could establish cutoff distances under variable observation scenarios (i.e., for varying satellite elevation angle e and receiving antenna height H), ideally arriving at simplified expressions that could serve as a more realistic rule-of-thumb than SP/FFZ formulas. Third, although we have demonstrated the importance of remote FZ only for a near-surface setup, in principle such sensitivity should persist even for antennas set up high above the surface, as the Rayleigh criterion for coherent scattering, $ks_H \sin e < 1$, does not involve the average height H, only the surface height standard deviation s_H. Fourth, further consideration for random surface roughness is justified, as it is known for enlarging the incoherent scattering footprint; conversely, we conjecture that it would cause the coherent scattering footprint to shrink.

IV. Conclusion

Although the specular point (SP) and the first Fresnel zone (FFZ) are often assumed to represent the footprint of a coherent reflection, we have demonstrated experimentally and with simulations that GPS multipath SNR observations exhibit significant sensitivity to perturbations originating elsewhere on the reflecting surface. The larger footprint is partially owed to the reception conditions under which a coherent reflection is left to interfere constructively and destructively with the direct or line-of-sight (LOS) propagation.

Such a more thorough footprint characterization has obvious implications for the calibration and validation (C&V) of GPS multipath reflectometry (GPS-MR) retrievals and their use for the C&V of other sensors. *In situ* sampling needs to occur over a larger area than otherwise thought by assuming that just the FFZ is involved. The sensitivity kernel also implies wider obstruction clearance requirements for new GPS-MR site installations. This understanding helps avoiding null results or statistically

insignificant correlations when comparing GPS-MR retrievals to other sensors.

Other than substantiating the footprint involved in SNR-based GPS-MR, the finite-frequency effects here demonstrated—unanticipated in Geometrical Optics (GO), as it assumes infinitesimal wavelength—suggest the possibility of overcoming the diffraction limit in GPS-R and performing sub-Fresnel imaging via GPS diffractive reflectometry (GPS-DR), i.e., to map out surface scattering features smaller than the FFZ.

REFERENCES

[1] T. E. Ochsner, M. H. Cosh, R. H. Cuenca, W. A. Dorigo, C. S. Draper, Y. Hagimoto, Y. H. Kerr, E. G. Njoku, E. E. Small, and M. Zreda, "State of the art in large-scale soil moisture monitoring," *Soil Sci. Soc. Amer. J.*, vol. 77, no. 6, p. 1888, 2013.

[2] W. T. Crow, A. A. Berg, M. H. Cosh, A. Loew, B. P. Mohanty, R. Panciera, P. de Rosnay, D. Ryu, and J. P. Walker, "Upscaling sparse ground-based soil moisture observations for the validation of coarse-resolution satellite soil moisture products," *Rev. Geophys.*, vol. 50, no. 2, Apr. 2012.

[3] D. Desilets and M. Zreda, "Footprint diameter for a cosmic-ray soil moisture probe: Theory and Monte Carlo simulations: Footprint diameter for a cosmic-ray soil moisture probe," *Water Res. Res.*, vol. 49, no. 6, pp. 3566–3575, Jun. 2013.

[4] S. Jin, E. Cardellach, and F. Xie, *GNSS Remote Sensing: Theory, Methods and Applications*. New York, NY: Springer-Verlag, 2013.

[5] V. U. Zavorotny, S. Gleason, E. Cardellach, and A. Camps, "Tutorial on remote sensing using GNSS bistatic radar of opportunity," *IEEE Geosci. Remote Sens. Mag.*, vol. 2, no. 4, pp. 8–45, Dec. 2014.

[6] K. M. Larson and E. E. Small, "Using GPS to study the terrestrial water cycle," *Eos Trans. Amer. Geophys. Union*, vol. 94, no. 52, pp. 505–506, Dec. 2013.

[7] R. N. Treuhaft, S. T. Lowe, C. Zuffada, and Y. Chao, "2-cm GPS altimetry over crater lake," *Geophys. Res. Lett.*, vol. 28, no. 23, p. 4343, 2001.

[8] M. Martin-Neira, P. Colmenarejo, G. Ruffini, and C. Serra, "Altimetry precision of 1 cm over a pond using the wide-lane carrier phase of GPS reflected signals," *Can. J. Remote Sens.*, vol. 28, no. 3, pp. 394–403, Jun. 2002.

[9] A. Helm, G. Beyerle, and M. Nitschke, "Detection of coherent reflections with GPS bipath interferometry," *arXiv:physics/0407091*, Jul. 2004.

[10] M. Belmonte Rivas and M. Martin-Neira, "Coherent GPS reflections from the sea surface," *IEEE Geosci. Remote Sens. Lett.*, vol. 3, no. 1, pp. 28–31, Jan. 2006.

[11] A. M. Semmling, G. Beyerle, R. Stosius, G. Dick, J. Wickert, F. Fabra, E. Cardellach, S. Ribó, A. Rius, A. Helm, S. B. Yudanov, and S. D'Addio, "Detection of arctic ocean tides using interferometric GNSS-R signals," *Geophys. Res. Lett.*, vol. 38, no. 4, pp. 38–41, Feb. 2011.

[12] F. Fabra, E. Cardellach, A. Rius, S. Ribo, S. Oliveras, O. Nogues-Correig, M. Belmonte Rivas, M. Semmling, and S. D'Addio, "Phase altimetry with dual polarization GNSS-R over sea ice," *IEEE Trans. Geosci. Remote Sens.*, vol. 50, no. 6, pp. 2112–2121, Jun. 2012.

[13] A. Kavak, W. J. Vogel, and G. Xu, "Using GPS to measure ground complex permittivity," *Electron. Lett.*, vol. 34, no. 3, pp. 254–255, 1998.

[14] K. D. Anderson, "Determination of water level and tides using interferometric observations of GPS signals," *J. Atmospheric Ocean. Technol.*, vol. 17, no. 8, pp. 1118–1127, Aug. 2000.

[15] K. Yu, W. Ban, X. Zhang, and X. Yu, "Snow depth estimation based on multipath phase combination of GPS triple-frequency signals," *IEEE Trans. Geosci. Remote Sens.*, vol. 53, no. 9, pp. 5100–5109, Sep. 2015.

[16] M. Ozeki and K. Heki, "GPS snow depth meter with geometry-free linear combinations of carrier phases," *J. Geod.*, vol. 86, no. 3, pp. 209–219, Sep. 2011.

[17] K. M. Larson and E. E. Small, "Normalized microwave reflection index: A vegetation measurement derived from GPS networks," *IEEE J. Sel. Top. Appl. Earth Obs. Remote Sens.*, vol. 7, no. 5, pp. 1501–1511, May 2014.

[18] N. Rodriguez-Alvarez, X. Bosch-Lluis, A. Camps, A. Aguasca, M. Vall-llossera, E. Valencia, I. Ramos-Perez, and H. Park, "Review of crop growth and soil moisture monitoring from a ground-based instrument implementing the interference pattern GNSS-R technique," *Radio Sci.*, vol. 46, pp. 1–11, Oct. 2011.

[19] M. Totzeck, "Interferometry," in *Springer Handbook of Lasers and Optics*, F. Träger, Ed. Berlin, Germany: Springer, 2012, pp. 1255–1283.

[20] A. R. Thompson, J. M. Moran, and George W. Swenson Jr, *Interferometry and Synthesis in Radio Astronomy*. Weinheim, Germany: Wiley, 2008.

[21] A. Romero-Wolf, S. Vance, F. Maiwald, E. Heggy, P. Ries, and K. Liewer, "A passive probe for subsurface oceans and liquid water in Jupiter's icy moons," *Icarus*, vol. 248, pp. 463–477, Mar. 2015.

[22] Y. A. Kravtsov, *Geometrical Optics in Engineering Physics*. Oxford, UK: Alpha Science, 2005.

[23] R. Notarpietro, S. De Mattia, M. Campanella, Y. Pei, and P. Savi, "Detection of buried objects using reflected GNSS signals," *EURASIP J. Adv. Signal Process.*, vol. 2014, no. 1, p. 132, 2014.

[24] A. Santamaría-Gómez, C. Watson, M. Gravelle, M. King, and G. Wöppelmann, "Levelling co-located GNSS and tide gauge stations using GNSS reflectometry," *J. Geod.*, pp. 1–18, Dec. 2014.

[25] S. Yan, Z. Li, K. Yu, and K. Zhang, "GPS-R L1 interference signal processing for soil moisture estimation: An experimental study," *EURASIP J. Adv. Signal Process.*, vol. 2014, no. 1, p. 107, 2014.

[26] E. Hecht, *Optics*, 4th ed. Reading, MA, USA: Addison-Wesley, 2001.

[27] J. Tong, F. A. Dahlen, G. Nolet, and H. Marquering, "Diffraction effects upon finite-frequency travel times: A simple 2-D example," *Geophys. Res. Lett.*, vol. 25, no. 11, pp. 1983–1986, Jun. 1998.

[28] R. Montelli, G. Nolet, F. A. Dahlen, G. Masters, E. R. Engdahl, and S.-H. Hung, "Finite-frequency tomography reveals a variety of plumes in the mantle," *Science*, vol. 303, no. 5656, pp. 338–343, Jan. 2004.

[29] F.-C. Lin and M. H. Ritzwoller, "Empirically determined finite frequency sensitivity kernels for surface waves: Empirical sensitivity kernels for surface waves," *Geophys. J. Int.*, vol. 182, no. 2, pp. 923–932, Jul. 2010.

[30] P. Roux, C. Marandet, B. Nicolas, and W. A. Kuperman, "Experimental measurement of the acoustic sensitivity kernel," *J. Acoust. Soc. Amer.*, vol. 134, no. 1, p. EL38, 2013.

[31] H. D. Hristov, *Fresnel Zones in Wireless Links, Zone Plate Lenses and Antennas*. Norwood, MA, USA: Artech House, 2000.

[32] C. D. Rodgers, *Inverse Methods for Atmospheric Sounding: Theory and Practice*. Singapore: World Scientific, 2000.

[33] A. Fichtner, *Full Seismic Waveform Modelling and Inversion*. Berlin, Germany: Springer, 2010.

[34] S. H. Byun, G. A. Hajj, and L. E. Young, "Development and application of GPS signal multipath simulator," *Radio Sci.*, vol. 37, no. 6, p. 1098, Nov. 2002.

[35] J. Li, G. Taylor, D. Kidner, and M. Ware, "Prediction and visualization of GPS multipath signals in urban areas using LiDAR Digital Surface Models and building footprints," *Int. J. Geogr. Inf. Sci.*, vol. 22, no. 11–12, pp. 1197–1218, Nov. 2008.

[36] V. U. Zavorotny and A. G. Voronovich, "Scattering of GPS signals from the ocean with wind remote sensing application," *IEEE Trans. Geosci. Remote Sens.*, vol. 38, no. 2, pp. 951–964, Mar. 2000.

[37] G. A. Hajj and C. Zuffada, "Theoretical description of a bistatic system for ocean altimetry using the GPS signal," *Radio Sci.*, vol. 38, no. 5, p. 1089, Oct. 2003.

[38] F. G. Nievinski and K. M. Larson, "Forward modeling of GPS multipath for near-surface reflectometry and positioning applications," *GPS Sol.*, vol. 18, no. 2, pp. 309–322, Apr. 2014.

[39] Y. Georgiadou and A. Kleusberg, "On carrier signal multipath effects in relative GPS positioning," *Manuscripta Geod.*, vol. 13, no. 3, pp. 172–179, 1988.

[40] J. J. Spilker, Jr. and A. J. Vandierendonck, "Proposed new L5 civil GPS codes," *Navigation*, vol. 48, no. 3, pp. 135–143, 2001.

[41] S. Tabibi, F. G. Nievinski, T. van Dam, and J. F. G. Monico, "Assessmentof modernized GPS L5 SNR for ground-based multipath reflectometry applications," *Adv. Space Res.*, vol. 55, no. 4, pp. 1104–1116, doi:10.1016/j.asr.2014.11.019

[42] E. Krantz, S. Riley, and P. Large, "The design and performance of the Zephyr geodetic antenna," in *Proc. ION GPS*, 2001, Salt Lake City, UT, USA, pp. 1942–1951.

[43] M. Smyrnaios, S. Schn, and M. Liso, "Multipath propagation, characterization and modeling in GNSS," in *Proc. Geodetic Sci. Obs., Model. Appl.*, S. Jin, Ed. InTech, Rijeka, Croatia, 2013, pp. 99–124.

[44] P. H. Pathak and R. J. Burkholder, "High-frequency methods," in *Scattering: Scattering and Inverse Scattering in Pure and Applied Science*, 1 ed., vol. 1, 2 vols., E. R. Pike and P. C. Sabatier, Eds. San Diego, CA, USA: Academic Press, 2001, pp. 245–276.

[45] M. P. Clarizia, C. Gommenginger, M. Di Bisceglie, C. Galdi, and M. A. Srokosz, "Simulation of L-band bistatic returns from the ocean surface: A facet approach with application to ocean GNSS reflectometry," *IEEE Trans. Geosci. Remote Sens.*, vol. 50, no. 3, pp. 960–971, Mar. 2012.

[46] N. Pierdicca, L. Guerriero, R. Giusto, M. Brogioni, and A. Egido, "SAVERS: A simulator of GNSS reflections from bare and vegetated soils," *IEEE Trans. Geosci. Remote Sens.*, vol. 52, no. 10, pp. 6542–6554, Oct. 2014.
[47] T. Shijo, T. Itoh, and M. Ando, "Visualization of high frequency diffraction based on physical optics," *IEICE Trans. Electron.*, vol. 87, no. 9, pp. 1607–1614, Sep. 2004.
[48] F. G. Nievinski and K. M. Larson, "An open source GPS multipath simulator in Matlab/Octave," *GPS Sol.*, vol. 18, no. 3, pp. 473–481, Jul. 2014.
[49] N. Pinel and C. Bourlier, *Electromagnetic Wave Scattering from Random Rough Surfaces: Asymptotic Models. Hoboken, NJ, USA: Wiley*, 2013.
[50] D. B. Davidson, *Computational Electromagnetics for RF and Microwave Engineering, 2nd ed.* Cambridge, U.K.: Cambridge University Press, 2011.
[51] T. Takasu and A. Yasuda, "Development of the low-cost RTK-GPS receiver with an open source program package RTKLIB," in *Proc. Int. Symp. GPS/GNSS*, Jeju, Korea, pp. 4–6, 2009.
[52] JCGM, "Evaluation of measurement data—Guide to the expression of uncertainty in measurement," Joint Committee for Guides in Metrology, JCGM 100:2008, Sep. 2008.

Felipe Geremia-Nievinski received the B.E. from the Federal University of Rio Grande do Sul in Porto Alegre, RS, Brazil in 2005, the M.S.Eng. degree (geomatics engineering) from the University of New Brunswick in Fredericton, NB, Canada, in 2009, and the Ph.D. degree (aerospace engineering sciences) from the University of Colorado, Boulder, CO, USA in 2013.

From 2013 to 2015, he was a Postdoctoral Research Fellow with the Space Geodesy Study Group at São Paulo State University. In 2015, he joined the Federal Institute of Santa Catarina, SC, Brazil. Since 2016, he has been a Full-time Faculty Member at the Federal University of Rio Grande do Sul (Department of Geodesy), RS, Brazil. His current research interests include satellite geodesy and tropospheric modeling and reflectometric sensors for environmental applications. He is the author of more than 20 peer-reviewed articles and contributes as a reviewer in 15 journals.

Dr. Geremia-Nievinski was the Institute of Navigation Bradford W. Parkinson awardee for Outstanding Ph.D. Thesis in global navigation satellite systems in 2013 and the Science without Borders Young Talent Researcher Fellow from the Brazilian government in 2013−2015; he also received the NASA Earth System Science fellowship in 2012−2013, the American Geophysical Union Outstanding Student Paper Award in Fall 2010 (Cryosphere Sciences Focus Group) and 2008 (Geodesy Section), and was a Fulbright Program Recipient in 2008−2012.

Matheus Ferreira e Silva was born in Presidente Prudente, SP, Brazil. He is currently working toward the B.E. degree from São Paulo State University, Sao Paulo, Brazil.

Karen Boniface (M'15) received the Diploma in mechanical engineering from the University of Technology of Belfort-Montbéliard (UTBM), Sevenans, France, in 2005, the M.S. degree in fluid mechanics from the University of Chalmers, Göteborg, Sweden, in 2006, and the Ph.D. degree in geosciences from the University of Montpellier, Montpellier, France in 2009.

From 2010 to 2012, she was with Environment Canada with a grant from the *Natural Sciences and Engineering Research Council* of Canada (*NSERC*), where she was involved in global navigation satellite systems (GNSS) radio occultation reflected signals aspects. From 2012 to 2013, she was a Research Associate at the University of Colorado, CO, Boulder, USA. Since 2013, she joined ISTerre (*Institut des Sciences de la Terre*) in Grenoble, France, with a grant from the *French National Centre for Space Studies (CNES).* Her current research interests include the use of GNSS reflection (GNSS-R) techniques for Earth sciences applications and in particular snow measurements.

João Francisco Galera Monico received the B.Sc. degree in cartographic engineering from the Sao Paulo State University (UNESP) São Paulo, Brazil, in 1982, the M.Sc. degree in geodetic science from the Federal University of Paraná (UFPR), Curitiba, Paraná, Brazil in 1988, and the Ph.D. degree in space geodesy from the Univeristy of Nottingham, Nottingham, U.K., in 1995.

From 2005 to 2013, he was an Adjunct Professor at the Department of Cartography, Sao Paulo State University (UNESP) at Presidente Prudente in Brazil, where he was lecturing and researching topics related to GNSS, especially those related to geodesy, surveying, and atmospheric sciences, where since 2013, he has been a Researcher.